

Unique Domain for a Unique Target: Selective Inhibitors of Host Cell DDX3X to Fight Emerging Viruses

Valentina Riva, Anna Garbelli, Annalaura Brai, Federica Casiraghi, Roberta Fazi, Claudia I. Trivisani, Adele Boccuto, Francesco Saladini, Ilaria Vicenti, Francesco Martelli, Maurizio Zazzi, Simone Giannecchini, Elena Dreassi, Maurizio Botta, and Giovanni Maga*



Cite This: *J. Med. Chem.* 2020, 63, 9876–9887



Read Online

ACCESS |



Metrics & More

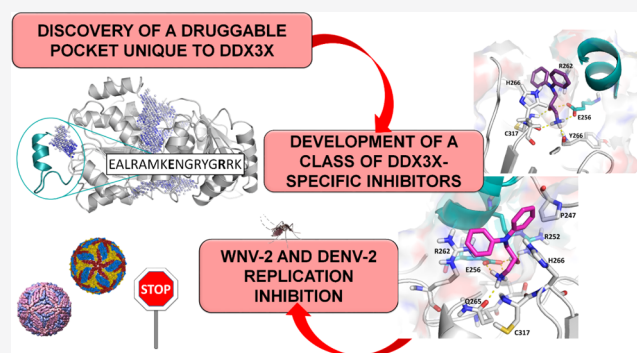


Article Recommendations



Supporting Information

ABSTRACT: Emerging viruses like dengue, West Nile, chikungunya, and Zika can cause widespread viral epidemics. Developing novel drugs or vaccines against specific targets for each virus is a difficult task. As obligate parasites, all viruses exploit common cellular pathways, providing the possibility to develop broad-spectrum antiviral agents targeting host factors. The human DEAD-box RNA helicase DDX3X is an essential cofactor for viral replication but dispensable for cell viability. Herein, we exploited the presence of a unique structural motif of DDX3X not shared by other cellular enzymes to develop a theoretical model to aid in the design of a novel class of highly selective inhibitors acting against such specific targets, thus limiting off-targeting effects. High-throughput virtual screening led us to identify hit compound **5**, endowed with promising antienzymatic activity. To improve its aqueous solubility, **5** and its two enantiomers were synthesized and converted into their corresponding acetate salts (compounds **11**, **12**, and **13**). *In vitro* mutagenesis and biochemical and cellular assays further confirmed that the developed molecules were selective for DDX3X and were able to suppress replication of West Nile and dengue viruses in infected cells in the micromolar range while showing no toxicity for uninfected cells. These results provide proof of principle for a novel strategy in developing highly selective and broad-spectrum antiviral molecules active against emerging and dangerous viral pathogens. This study paves the way for the development of larger focused libraries targeting such domain to expand SAR studies and fully characterize their mode of interaction.



INTRODUCTION

Despite much social visibility and alertness to the impact of widespread viral epidemics, a significant number of emerging viral pathogens remain without effective treatment or cure. For example, no specific and effective pharmacological treatments are currently available for diseases caused by the dengue virus (DENV), West Nile virus (WNV), Japanese encephalitis virus (JEV), chikungunya virus (CHIKV), and Zika virus (ZIKV), while it is becoming clear that they pose an increasing global health threat and could eventually lead to sustained epidemics worldwide.¹

The current view of the infected cell as a “virocell”² reflects the notion that the metabolism of the infected cells is completely remodeled and redirected to produce new viral particles. The extent of such reprogramming has been well illustrated by transcriptome- and proteome-level studies in cells infected by different viruses, showing that the limited number of viral proteins transcribed from the viral mRNAs can interact with hundreds of cellular proteins, often located at the nodes of complex metabolic networks.³ A key observation stemming from these studies is that many different viruses rely on the

same cellular proteins for modulating the host cell response. One of these proteins is the human X-linked DEAD-box protein 3 (DDX3X).

DDX3X is involved in different cellular pathways (translation, transcription, RNA decay, ribosome biogenesis).^{4,5} It participates in cell cycle control, apoptosis, oncogenic transformation, cell migration, and hypoxia, and is overexpressed in a large number of cancers and has been proposed as a novel target for the development of anticancer therapeutics.^{6–8} DDX3X inhibitors have been identified with specific anticancer activities in mouse models, without exerting long-term toxic effects on the animals.^{9,10} Given the high homology between human and murine DDX3X (98.6%), these results strongly support the notion that inhibiting DDX3X should not

Received: June 17, 2020

Published: July 30, 2020



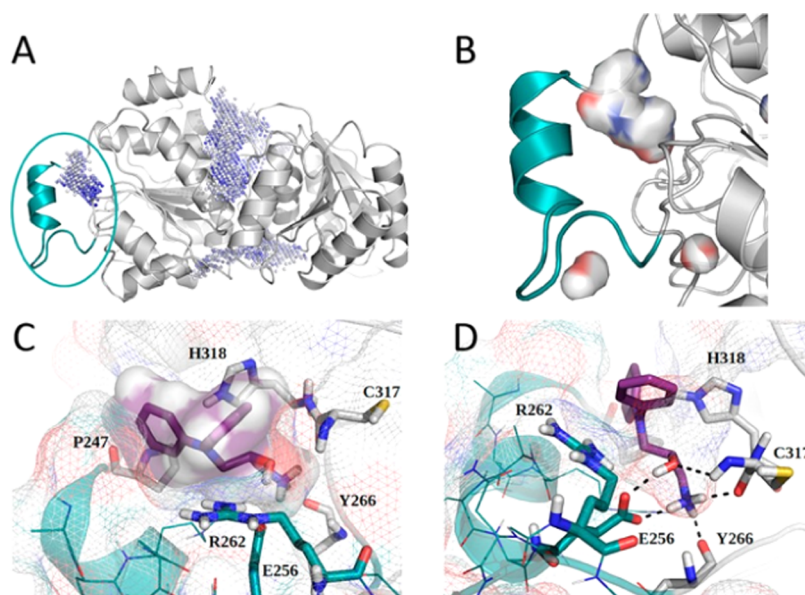


Figure 1. Molecular modeling of the inhibitor-binding pocket. (A) Pockets identified by PockerPicker are represented in dots. The unique motif UM (cyan) with the adjacent pocket is circled. (B) Zoomed-in view of the little pocket around the unique motif (cyan). (C, D) Two different orientations of compound 5 docked pose showing, respectively, its particular shape profile and its specific polar interactions with residues within the motif. The templates used were PDB codes 2DB3 and 2I4I.

result in major adverse effects in humans also, providing proof of principle that DDX3X inhibitors can be used to selectively target cancer with minimal toxicity for normal cells.

DDX3X is also an essential host factor for the replication of viruses belonging to different families, such as *Herpesviridae*, *Retroviridae*, *Flaviviridae*, *Poxviridae*, and *Caliciviridae*, where it plays different roles in their life cycle.^{11,12} DDX3X participates also in the host innate immunity. It has been shown to interact with and regulate the protein kinases IKK ϵ and TBK-1, involved in IFN- β production, as well as to regulate the NF- κ B-dependent inflammatory response.¹³ However, how DDX3X activity is coordinated in the different branches of the innate immune response and to what extent its role is essential in the global antiviral response of the cells are still not completely understood. In recent years, different groups, including ours, have extensively studied DDX3X as a target to control viral infections and developed small-molecule inhibitors targeting both the ATP- and RNA-binding sites of DDX3X.¹⁴ In particular, we have identified an RNA-competitive inhibitor targeting the nucleic acid-binding cleft of DDX3X, which was able to block the replication of human immunodeficiency virus type 1 (HIV-1) as well as hepatitis C virus (HCV), DENV, and WNV, and this despite the potential antiviral role of DDX3X in innate immunity.¹⁵ Preliminary *in vivo* studies in rats showed no toxic effects for this compound.¹⁵ This suggests that targeting DDX3X could be a powerful method to halt the replication of different viruses.

However, to further develop such compounds for human use, it is of paramount importance to endow them with chemical and structural features able to guarantee an absolute selectivity for DDX3X only. This has proven a challenging task, due to the significant similarity both from a sequence and a structural point of view, in the ATP- and RNA-binding sites among the members of the DEAD-box family of RNA helicases.¹⁶ The name of the family derives from the Walker B motif II D-E-A-D (Asp-Glu-Ala-Asp), which contains the catalytic residues essential for ATP hydrolysis. In all DEAD-

box helicases characterized to date, the ATPase and RNA helicase motifs involved in RNA substrate binding and hydrolysis are distributed in two RecA-like subdomains. Also in DDX3X, all of the 12 canonical motifs common to all members of the DEAD-box RNA helicase family are present in both domains (domain 1 and domain 2, from the N- to C-terminal) connected via a short flexible linker.¹¹ DEAD-box helicases, including DDX3X, also contain additional specific motifs. The Q-motif establishes specific contacts with the adenine base of ATP, while two additional motifs, Ib (also termed the GG-motif) and IVa (or the QxxR-motif), are involved in specific contact with the RNA substrate.^{14,17} In DDX3X, an additional ATP-interacting domain (ABL, aa 135–168) is involved in RNA stimulation of ATP hydrolysis.¹⁸

In addition to all of the canonical conserved domains, DDX3X has been shown to possess a unique insertion, hence named the “unique motif” (sequence -ALRAMKENGRYGRRK- aa 250–264), between motif I (Walker A), which is involved in ATP binding, and motif Ia, which is part of the RNA-binding domain. Unfortunately, all of the available crystal structures of DDX3X do not allow us to have detailed information about this unique motif. In the structure reported by Schütz and collaborators,¹⁹ the DDX3X crystal lacks bound RNA, thus representing the “open” conformation of the enzyme and making it difficult to determine the precise nature of the contacts between the unique motif (UM) residues and the nucleic acid lattice. Vice versa, in the more recent structure reported by Song and Ji,²⁰ active conformation, the UM region is not present probably because of its very mobile nature, which makes the crystallization a difficult task.

Despite the scarce structural information, such insertion represents a very attractive target since it is not present in other human protein members of the DEAD-box family,²¹ and Basic Local Alignment Search Tool (BLAST) analysis indicated that no other human protein shares significant homology with the amino acidic sequence of the UM.

We have previously shown that deleting this short motif affected the RNA helicase activity of DDX3X, by reducing its affinity for the nucleic acid, and that blocking this domain with a peptide reduced HIV-1 replication in infected cells.¹¹ These results suggested that inhibitors targeting the UM could be highly selective for DDX3X, due to the absence of such domains in other human proteins, and might retain the ability to suppress viral replication.

In light of these preliminary data, we decided to make the UM the focus of a novel strategy to develop highly selective and broad-spectrum antivirals, by designing small molecules specifically targeting this unique DDX3X motif.

RESULTS

Molecular Modeling. Structure-guided drug design is a powerful approach to develop molecules specifically tailored to a target. However, the reliability of such an approach relies on the availability of high-resolution structures of the desired target. Unfortunately, at the time of the starting of this project, no structures of DDX3X in its active conformation were available. Thus, to overcome this limitation and to study the human DDX3X active closed conformation, we built a homology model using as the first template the crystal structure of *Drosophila* Vasa DEAD-box helicase (PDB code: 2DB3), which is cocrystallized with AMPPNP and an RNA fragment and shows a 44% sequence homology with DDX3X. Since the DDX3X unique motif is missing in the 2DB3 structure, the crystal structure of DDX3X in the open conformation (PDB code: 2I4I) was chosen as the second template to fill the missing region. The homology model was built using the software PRIME.

The recent structure reported by Song and Ji²⁰ of DDX3X in its active conformation does not contain the UM region. Hence, we decided to build the UM homology model (Figure S1) using the software PRIME and as the template the crystal structure of DDX3X in the open conformation (PDB code: 2I4I). The root-mean-square deviation (RMSD) calculated between DDX3X domains containing the UM region in the homology model and in the crystal structure is 1.03 Å, indicating the reliability of the modeling approach. Moreover, as reported by Song and Ji, our homology model represents the post-unwound state of the DDX3X protein. Our approach has obvious limitations, being based on homology modeling, even though developed with the most accurate tools and appropriate templates available. However, it represents the only available theoretical framework to start exploring the druggable properties of the UM subdomain of DDX3X.

Thus, starting from our homology model, using PocketPicker, a pymol plugin able to detect all of the possible pockets on a protein surface, we found a potential little pocket lined by the α -helix formed by the DDX3X unique motif (Figure 1A,B).

Since no molecules able to bind this pocket within the UM have ever been described, we performed a preliminary screening to search theoretically active scaffolds among two commercial libraries (Asinex Gold and Platinum consisting of 583 040 molecules) using two different docking programs. Molecules were first docked within our selected pocket using GLIDE with the high throughput virtual screening (HTVS) procedure, which allowed us to analyze a large number of molecules. From this analysis, we chose the best-scoring molecules (74 783: 20% of the total) to be processed in the next step.

Selected molecules were docked again within the pocket using the docking program GOLD (CHEMSCORE). The following parameters were used to detect the box grid for the docking study: cavity centered by atom Arg252, radius 9 Å. Docked molecules were then selected based on (i) score values above 23, (ii) the number of clusters generated (less than 7), and (iii) visual inspection. Because of the small and narrow properties of the pocket, a fair number of compounds were docked outside and so they were discarded. Among the molecules that passed the filter analysis and were docked inside the pocket (about 103), 10 compounds were finally selected as interesting, based on their chemical structures and their polar interactions into the active site.

Identification of Hit Compounds. These molecules were then tested for their ability to inhibit DDX3X RNA helicase activity in enzymatic assays. Table 1 lists the chosen compounds with their structures, docking scores, and antienzymatic activities.

We then used our theoretical homology model to formulate hypotheses on the kind of structural features that might account for their activity. A first group of these molecules (4, 8, and 10) was selected on the basis of hypothesized interesting polar interactions of the terminal amino group with three amino acids in the pocket (Glu256, Tyr266, Cys317). Another group of compounds (1, 2, 7) was selected considering the shape and the residues involved in the hydrophobic interactions that are Arg262, His318, and Pro247.

Based on our theoretical model, compound 5 was hypothesized to have an interesting shape that fits into the pocket like a “cap”. Remarkably, compound 5 is the only one among the selected molecules characterized by the presence of a hydroxyl group possibly able to interact with both Glu256 and Cys317 (Figure 1C,D). As shown in Figure 2, the visual analysis of the binding mode of compounds 1 and 7, characterized by the high score but inactive in the biochemical assay, showed that these molecules are not able to interact with Cys317, Tyr266, and Glu256. These last interactions characterize the binding mode of compounds 5, 11, and 13 and are probably responsible for their activity. To confirm the activity of this commercially available molecule, compound 5 was resynthesized as depicted in Scheme 1, and converted into the corresponding acetate salt (compound 11, Table 1). This simple synthetic modification provides a water-soluble derivative. Furthermore, the *R* and *S* enantiomers (compounds 12 and 13, Table 1) were synthesized as described in Scheme 1.

More in detail, epoxides 15a–c were produced starting from diphenylamine that was alkylated with racemic epichlorohydrin or with (*R*)-(–) or (*S*)-(+ epichlorohydrin. Propanolamines 5, 16a, and 16b were then obtained by reaction with gaseous ammonia and subsequent treatment with acetic acid to furnish the corresponding water-soluble acetate salts 11–13 (Scheme 1).

All three compounds showed greatly improved potencies with respect to compound 5 (Figure S3), being able to suppress DDX3X helicase activity in the low nanomolar range, likely due to improved solubility (Table 1). These compounds were used for all of the subsequent experiments, as described below.

The modeling study predicted that compound 5 could establish polar interactions with the amino acids Glu256, Cys317, and Tyr266, and hydrophobic interactions with Arg262, His318, and Pro247. In particular, the docking

Table 1. Inhibitory Activity and Docking Score of Selected Compounds Targeting the UM of DDX3X

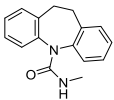
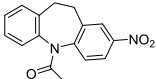
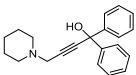
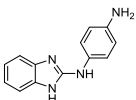
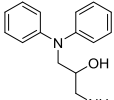
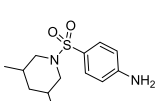
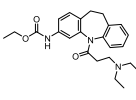
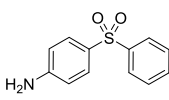
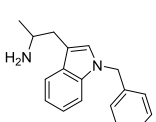
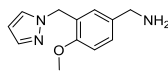
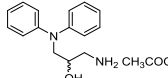
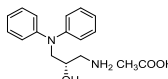
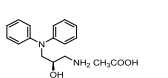
Cmpd ID	Chemical structure	ID _{50a} (μM)	Docking score (CHEMSCORE)	QP logS
1		n.a	25.22	-3.519
2		n.a	24.76	-3.852
3		n.a	25.15	-4.276
4		n.a	24.83	-2.896
5		0.7±0.2	24.68	-2.126
6		n.a	25.82	-3.355
7		n.a	27.27	-5.331
8		200±30	24.94	-2.424
9		n.a	25.68	-3.437

Table 1. continued

Cmpd ID	Chemical structure	ID _{50a} (μM)	Docking score (CHEMSCORE)	QP logS
10		n.a	25.86	-1.632
11		0.002 ± 0.0005	24.68	-2.126
12		0.007 ± 0.0001	24.28	-2.126
13		0.006 ± 0.0001	21.65	-2.126

^aID₅₀, inhibitor concentration reducing by 50% the enzyme activity. Values are the mean of three independent replicates ± SD.

analysis allowed us to hypothesize that the Glu256 and Arg262 residues, located at the N- and C-terminal sides of the UM sequence, respectively, are the major residues responsible for compound **5** binding. As all of these structural considerations are based on theoretical assumptions stemming from our homology modeling, it was necessary to experimentally validate them. Thus, the compounds listed above were selected for further investigation.

Glu 256 is Essential for the RNA Helicase Activity of DDX3X. In an attempt to obtain experimental evidence of the reliability of the molecular modeling predictions, the amino acidic residues Glu256 and Arg262 of DDX3X were changed into Ala by site-directed mutagenesis to generate, respectively, the two single E256A and R262A mutants and the double E256A/R262A mutant (Figure S2). Next, to evaluate the impact of these mutations on the enzymatic activity, the mutated enzymes were tested for their RNA helicase activities in a fluorescence resonance energy transfer (FRET)-based assay, and the kinetic parameters for the reaction are reported in Table 2.

The E256A substitution had the greatest impact on the enzymatic efficiency, causing a 10.8-fold reduction of the k_{cat}/K_m value for RNA unwinding, with respect to wild-type DDX3X. The R262A mutation also reduced the k_{cat}/K_m value by 4.4-fold with respect to the wild-type enzyme. Combining the two mutations did not result in an additive effect and the double mutant showed an intermediate phenotype (7.4-fold reduction in the k_{cat}/K_m value with respect to the wild type), suggesting that the effect of the E256A mutation was not changed by the presence of the additional R262A substitution.

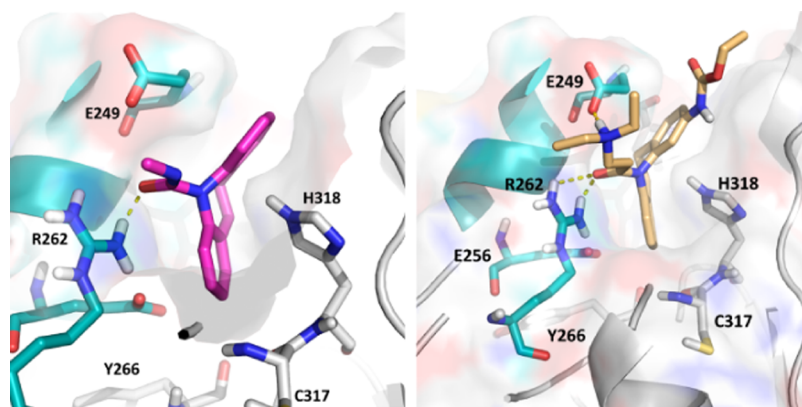
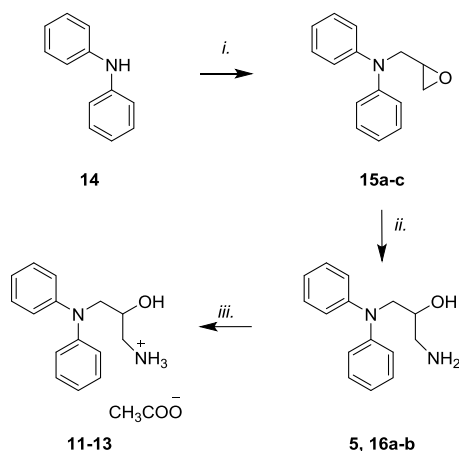


Figure 2. In magenta is reported the binding mode of compound 1. The compound establishes a hydrogen bond with Arg262 and is involved in a π - π stacking interaction with His266. Compound 7 is reported in yellow and is involved in hydrogen bonds with Arg262 and Glu249 and in π - π stacking interactions with His266.

Scheme 1. Synthesis of Compounds 11–13^a



^aReagents and conditions. (i) NaNH₂, benzene, 12 h, reflux; (ii) NH₃(g), DCM, 72 h, from -78 °C to r.t.; and (iii) CH₃COOH, DCM, 6 h, r.t.

Table 2. Kinetic Parameters for the RNA Helicase Activity of DDX3X Wild Type and the DDX3X(E256A), DDX3X(R262A), and DDX3X(E256A/R262A) Mutants^a

enzyme	K_m (RNA) (μM)	k_{cat} (FU ^b /min)	k_{cat}/K_m (μM^{-1} , FU/min)	-fold reduction ^c
wild type	0.5 ± 0.1	1146 ± 22	2278	1
E256A	0.6 ± 0.2	126 ± 10	210	10.8
R262A	9 ± 2	4794 ± 62	522	4.4
E256A/R262A	0.6 ± 0.25	148 ± 70	307	7.4

^aKinetic parameters K_m and k_{cat} were calculated as described in the Experimental Section; values represent the mean of three independent experiments ±S.D. ^bFU, arbitrary fluorescence emission units. ^cRatio $k_{\text{cat}}/K_m(\text{wt})/k_{\text{cat}}/K_m(\text{mut})$.

Table 3. Inhibition of the RNA Helicase Activity of DDX3X Wild Type and the DDX3X(E256A) and DDX3X(R262A) Mutants

compound	wild type ID ₅₀ , μM ^a	E256A ID ₅₀ , μM (-fold resistance) ^b	R262A ID ₅₀ , μM (-fold resistance)
11	0.002 ± 0.0005	73 ± 10 (36 500)	0.001 ± 0.0003 (0.5)
13	0.007 ± 0.0001	0.3 ± 0.1 (43)	0.004 ± 0.002 (0.6)

^aID₅₀, concentration of the compounds giving 50% inhibition of the activity measured for the respective enzyme in the absence of an inhibitor. Values were calculated as described in the Experimental Section and represent the mean of three independent experiments ±S.D. ^bRatio ID₅₀(mut)/ID₅₀(wt).

The single mutants were also compared for their ATPase activities. As shown in Figure S4, the E256A mutant showed comparable activity with respect to the wild-type enzyme, while the ATPase activity of the R262A mutant was reduced, similar to the double E256A/R262A mutant. In summary, these results indicated that the residue Glu256 is essential for the RNA helicase, but not for the ATPase activity of DDX3X, while Arg262 plays an ancillary role, likely coupling ATP hydrolysis to RNA unwinding. These results agree with previously published data indicating a role of the DDX3X UM in substrate binding and highlighting the central role of the residue Glu256 in this motif for RNA interaction.¹¹

Glu 256 is the Major Determinant for the Interaction of the UM Compounds with the DDX3X Unique Motif.

Next, compounds 11 and 13, designed as described above and hypothesized based on our theoretical *in silico* docking studies to interact with the mutated residues, were tested for their ability to inhibit the RNA helicase activity of DDX3X wild-type and mutant proteins. Even though the racemic compound 11 and its two enantiomers (compounds 12 and 13) showed comparable activities, as reported in Table 1, we chose to test 11 and one of the two enantiomers to further confirm our data. As shown in Table 3, the E256A substitution caused a reduction of the inhibitory potencies of compounds 11 and 13 of 36 500- and 43-fold, respectively. On the other hand, the mutation R262A did not significantly change the inhibitory potencies of the compounds, with respect to the wild-type enzyme. Thus, the residue Glu256 appeared as a major determinant for inhibitor binding.

These results were in good agreement with the molecular modeling and the kinetic analysis (Table 2), which indicated that Glu256 provides essential interactions of DDX3X with its RNA substrate. The binding of the inhibitor to this key residue can be hypothesized to disrupt those interactions, providing a

possible structural basis for the selectivity of the mechanism of action of our compounds.

Selectivity and Antiviral Activity of UM Compounds.

To further prove the specificity of inhibition of the selected compounds toward DDX3X, inhibition assays were performed with three RNA helicases: the DEAD-box RNA helicase family members human DDX1 and plant STRS2 from *Arabidopsis thaliana*, and the DExH-family viral NS3 RNA helicase of HCV. As shown in Table 4, all of the compounds tested

Table 4. Inhibition of the RNA Helicase Activity of Human DDX1, Arabidopsis STRS2, and HCV NS3^a

compound	DDX1 ID ₅₀ , μM ^a (-fold selectivity) ^b	STRS2 ID ₅₀ , μM (-fold selectivity)	NS3 ID ₅₀ , μM (-fold selectivity)
11	18 ± 1.202 (9000)	>100 (>50 000)	>100 (>50 000)
13	58 ± 4.5 (8285)	>100 (>10 000)	>100 (>10 000)

^aID₅₀, 50% inhibitory concentration. Values were calculated as described in the Experimental Section and represent the mean of three independent experiments ± S.D. ^bRatio ID₅₀/ID₅₀ (wt DDX3X) and the ID₅₀ (wt DDX3X) values used were those reported in Table 1.

inhibited DDX1 with potencies almost four orders of magnitude lower than toward DDX3X (selectivity ≈9000-fold) and were completely inactive against STRS2 and NS3, confirming the high selectivity of inhibition for DDX3X. Again, these results provide support to our theoretical framework, indicating that the desired selectivity was apparently achieved.

Finally, compounds 11, 12, and 13 were tested for their ability to reduce WNV and DENV replication on Huh-7 cells. As reported in Table 5, compound 11 and its enantiomers 12

Table 5. Antiviral Activities and Cytotoxicity of Selected Compounds Against DENV and WNV^a

Cpd ID	IC ₅₀ ^b (DENV) (μM)	IC ₅₀ ^b (WNV) (μM)	CC ₅₀ ^{c,d} (μM)	CC ₅₀ ^{c,e} (μM)
#11	7.9 ± 3.3	2.3 ± 0.6	100 ± 11.3	>100
#12	12.6 ± 5.4	0.90 ± 0.20	120 ± 18.0	>100
#13	6.3 ± 5.8	0.88 ± 0.10	79 ± 11.8	>100
ribavirin	4.0 ± 0.6	91.5 ± 5	>100	>100

^aData represent mean + standard deviation of three experiments. ^bIC₅₀: half-maximal inhibitory concentration. ^cCC₅₀: half-maximal cytotoxic concentration. ^dCalculated using the CellTiter-Glo kit. ^eCalculated using the 3-(4,5-dimethylthiazol-2-yl)-2,5-diphenyltetrazolium bromide (MTT) kit; ribavirin was used as a reference compound.

and 13 showed promising antiviral activities in the micromolar range, resulting in IC₅₀ values comparable to (DENV) or even significantly lower (WNV) than those shown by the broad-spectrum antiviral ribavirin, without significant cytotoxicity (see also Figures S5 and S6).

DISCUSSION AND CONCLUSIONS

In this work, we attempted to develop a theoretical framework, based on a homology model of the human DDX3X in its closed conformation, to explore the possibility of developing molecules targeting a unique structural domain of the protein. The main aim of our work was to provide proof of principle for a strategy potentially leading to the development of small molecules able to couple broad-spectrum antiviral activity with absolute selectivity for their molecular target. Such a seemingly

paradoxical goal (broad-spectrum activity vs high selectivity for the target), in fact, could be in principle achieved by exploiting a specific cellular target, in our case the RNA helicase DDX3X, identifying a unique structural domain present only in the target, the UM domain of this study, and implementing molecular modeling, *in silico* drug design, and medicinal chemistry techniques, to design compounds specifically tailored on such a unique structural domain. An obvious limitation of our work is the fact that no high-resolution structures for the UM are presently available. We tried to overcome this limitation by developing a homology model using the best templates currently available. The coherence of our homology-built model with the most recent crystal structure of DDX3X in its active conformation was very high, assuring us on the reliability of our approach. Our hypothesized mode of binding was tested by *in vitro* mutagenesis and biochemical assays, whose results further corroborated the theoretical model proposed here, by confirming the selectivity of the designed molecules. Finally, cellular assays confirmed the antiviral activity as predicted.

A limited number of broad-spectrum antivirals targeting different families of viruses (RNA viruses, DNA viruses, and retroviruses) have been reported in the scientific literature up to now and only very few targeting cellular proteins.^{22–24} However, none of these compounds have been rationally designed against its target, with the specific aim of achieving optimal selectivity. Indeed, the main drawback of targeting a cellular protein is the possibility of unwanted side effects, either through the inhibition of the protein itself or by off-targeting of the drug toward other cellular enzymes. This problem is well known in the field of anticancer chemotherapy. For example, imatinib (also known as STI571 or Gleevec), is one of the most successful molecular targeted chemotherapeutics currently used in cancer therapy. This molecule was rationally designed to target the ATP-binding site of the tyrosine kinase ABL, but it was subsequently shown to interact also with other targets, most notably the receptor tyrosine kinases KIT and platelet-derived growth factor receptor (PDGFR),²⁵ thus failing to achieve the desired selectivity.

The cellular ATPase/RNA helicase DDX3X is considered an attractive molecular target for chemotherapy, since several studies indicated that inhibiting DDX3X can have therapeutic efficacy both against cancer and viral infections, without significant toxicity. In fact, as previously demonstrated by us, DDX3X inhibitors were very well tolerated in rats and mice.^{15,26} This is likely because DDX3X is part of a family of more than 50 related RNA helicases, which can have overlapping compensatory roles in cell metabolism.¹⁶ DDX3X is required for the replication of several viruses, including HIV-1, HCV, JEV, DENV, and WNV,^{27–29} and over the last few years, several molecules were developed by our group against DDX3X, providing proof of principle for its exploitation as a valuable new target for broad-spectrum antiviral chemotherapy.¹⁵ However, the significant similarity both from a sequence and a structural point of view, in the ATP- and RNA-binding sites among the members of the DEAD-box family of RNA helicases,¹⁶ makes it difficult to achieve absolute selectivity for DDX3X only by conventional drug design, leaving the problem of possible off-targeting effects still open.

The UM series of compounds described here represent the first class of inhibitors of the human helicase DDX3X, rationally designed to specifically recognize a unique motif

(sequence ALRAMKENGGRYGRRK- aa 250–264) of a unique target (DDX3X). This unique motif is not shared among other DExD-box proteins, nor with other human proteins. These molecules also showed no toxicity in cells and a considerable antiviral effect, being able to suppress the replication of WNV and DENV-2 viruses in infected cells.

ZIKV, DENV, CHIKV, and other viruses are transmitted to humans by the *Aedes aegypti* and *Aedes albopictus* mosquitoes. More than half of the world's population lives in areas where these mosquito species are present and climatic and human-caused changes can also expand the normal living niche of these animals.³⁰ The spread of the arthropod vectors and the increased movement of people among different geographical areas increase the risk of sudden outbreaks or even large epidemics caused by these mosquito-borne viruses and the number of infected people by the aforementioned viruses is indeed rising. For example, the worldwide incidence of DENV has risen 30-fold in the past 30 years, and more countries are reporting their first outbreaks of the disease (source: WHO). Consequently, it is important to develop new molecules acting against these pathogens for which no specific drugs are available to date.

Classically, strategies to control these arboviral infections aim at reducing the susceptibility to infection of the vector (reduced competence/transmission) or the host (antiviral drugs/vaccines). In this latter case, it would be greatly desirable to identify a unique target whose inhibition could counteract the infection of a wide range of arboviruses. In this respect, the cellular target DDX3X, central to the replication of different viruses, will offer the possibility to develop broad-spectrum antivirals, which are currently lacking in our antiviral arsenal.²⁸ The relevance and potential impact of the approach disclosed here are further enhanced by the fact that, besides being active against different viruses, an antiviral agent selectively targeting a unique host factor could have the additional advantage of overcoming the problem of drug resistance. In fact, a cell harboring a mutated version of the target protein will be more easily infected and thus either killed by the virus or by the host immune system, without gaining a fitness advantage. This, coupled with the low mutation rate of cellular proteins, could result in a very high genetic barrier toward drug resistance.

In conclusion, our results allow us to hypothesize that the unique domain of DDX3X could be used as a target for broad-spectrum antiviral drugs endowed with maximal selectivity. This study then paves the way for the development of larger focused libraries targeting this domain to expand SAR studies and fully characterize their mode of interaction.

EXPERIMENTAL SECTION

Homology Model. The homology model was obtained with the software PRIME (version 3.7)³¹ using the crystal structure of *Drosophila* Vasa DEAD-box helicase (PDB ID: 2DB3)³² as the first template and the open conformation of human DDX3X (PDB ID: 2I4I)³³ as the second template. This second template has been used to fill the sequence of 10 residues unique for the human DDX3X protein. All other parameters of PRIME tools are set as default values. The obtained model was energy minimized by the software MacroModel (version 10.5),³⁴ and it was also validated using the Ramachandran plot.

Docking Procedure. The Asinex Gold and Platinum databases were screened using GLIDE software (version 6.4)³⁵ with the HTVS procedure and GOLD docking tools program (version 3.2).³⁶ The genetic algorithm (GA) of GOLD allows for partial protein flexibility.

The box was centered on the Arg252 and has a radius of 9 Å. The ChemScore was chosen as the fitness function. The search efficiency was set to 100%. A total of 100 independent GA runs were performed, with a maximum number of 100 000 GA operations on a set of five islands with a population size of 200 individuals. The remaining GA parameters were kept to their default values.

Pictures of the modeled ligand–enzyme complexes, together with graphic manipulations, were rendered with the PyMOL package59 (version 1.5 [<http://www.pymol.org/>]).³⁷

Molecular graphics and analyses were performed with UCSF Chimera, developed by the Resource for Biocomputing, Visualization, and Informatics at the University of California, San Francisco, with support from NIH P41-GM103311 (version 1.14 [<http://www.rbvi.ucsf.edu/chimera/>]).³⁸

Methods. Reagents were obtained from commercial suppliers (Sigma-Aldrich and Alfa Aesar). All commercially available chemicals were used as purchased without further purification. CH₂Cl₂ and benzene were dried before use by distilling from calcium hydride or sodium/benzophenone. Anhydrous reactions were run under a positive pressure of dry N₂ or argon. Thin-layer chromatography (TLC) was carried out using Merck silica gel 60 F254 TLC plates. Chromatographic purifications were performed on columns packed with Merk 60 silica gel, 23-400 mesh, for the flash technique.

Instrumentation. All NMR spectra were recorded on a Bruker Avance DPX400 spectrometer at 400 MHz for ¹H NMR or 100 MHz for ¹³C NMR. Chemical shifts are reported relative to tetramethylsilane at 0.00 ppm. Mass spectra (MS) data were obtained using an Agilent 1100 LC/MSD VL system (G1946C) with a 0.4 mL/min flow rate using a binary solvent system 25 of 95:5 methyl alcohol/water. UV detection was monitored at 254 nm. Mass spectra were acquired in positive and negative mode scanning over the mass range. Microwave irradiation experiments were conducted using the CEM Discover Synthesis Unit (CEM Corp., Matthews, NC). For the quantitative analysis, a UV/LC-MS system was used. LC analysis was performed by the Agilent 1100 LC/MSD VL system (G1946C) (Agilent Technologies, Palo Alto, CA). Spectra were acquired over the scan range *m/z* 50–1500 using a step size of 0.1 u. The purity of the compounds (as measured by the peak area ratio) was >97%.

Chemistry. General Procedure for the Synthesis of Compounds 15a–c. Diphenylamine (1.1818 mmol) was added to a suspension of NaNH₂ (3.54 mmol) in anhydrous benzene. After 30 min, epichlorohydrin or (*R*)-(-)-epichlorohydrin or (*S*)-(+)-epichlorohydrin (1.18 mmol) was added, and the reaction was stirred at reflux for 12 h. After this time period, pH was adjusted to 7 with HCl 1 N and the mixture was extracted with EtOAc (3 × 25 mL). The organic layers were collected, washed with Brine, and dried over Na₂SO₄. The crude was purified by flash chromatography on silica gel using the opportune eluent.

***N*-(Oxiran-2-ylmethyl)-*N*-phenylaniline(15a).** Aspect colorless oil, *Y* = 89%. Eluent PE/EA = 8/2 ¹H NMR (400 MHz, CDCl₃) δ 7.26 (d, *J* = 8.1 Hz, 4H), 7.05 (d, *J* = 7.6 Hz, 4H), 6.96 (t, *J* = 7.8 Hz, 2H), 4.12–3.77 (m, 2H), 3.30–3.11 (m, 1H), 2.81–2.70 (m 1H), 2.61–2.52 (m, 1H). ¹³C NMR (101 MHz, CDCl₃) δ 149.34 (2C), 129.38 (4C), 122.73 (2C), 121.04 (4C), 53.02, 50.66, 46.18 ppm. MS: (ESI) *m/z* 226.0 (M + H)⁺.

***S*-(Oxiran-2-ylmethyl)-*N*-phenylaniline(15b).** Aspect colorless oil, *Y* = 85% PE/EA = 8/2 ¹H NMR (400 MHz, CDCl₃) δ 7.26 (d, *J* = 8.1 Hz, 4H), 7.05 (d, *J* = 7.6 Hz, 4H), 6.96 (t, *J* = 7.8 Hz, 2H), 4.12–3.77 (m, 2H), 3.30–3.11 (m, 1H), 2.81–2.70 (m 1H), 2.61–2.52 (m, 1H). ¹³C NMR (101 MHz, CDCl₃) δ 149.34 (2C), 129.38 (4C), 122.73 (2C), 121.04 (4C), 53.02, 50.66, 46.18 ppm. MS: (ESI) *m/z* 226.0 (M + H)⁺.

***R*-(Oxiran-2-ylmethyl)-*N*-phenylaniline(15c).** Aspect colorless oil, *Y* = 82% PE/EA = 8/2 ¹H NMR (400 MHz, CDCl₃) δ 7.26 (d, *J* = 8.1 Hz, 4H), 7.05 (d, *J* = 7.6 Hz, 4H), 6.96 (t, *J* = 7.8 Hz, 2H), 4.12–3.77 (m, 2H), 3.30–3.11 (m, 1H), 2.81–2.70 (m 1H), 2.61–2.52 (m, 1H). ¹³C NMR (101 MHz, CDCl₃) δ 149.34 (2C), 129.38 (4C), 122.73 (2C), 121.04 (4C), 53.02, 50.66, 46.18 ppm. MS: (ESI) *m/z* 226.0 (M + H)⁺.

General Procedure for the Synthesis of Compounds 5, 16a–c. Gaseous ammonia was bubbled into a solution of the opportune epoxide (0.1775 mmol) in dichloromethane (DCM), in a sealed tube. The corresponding mixture was stirred at room temperature for 72 h; then, volatiles were removed at reduced pressure, and the crude was purified by flash chromatography on silica gel (Purification Eluent: DCM/MeOH 9:1).

1-Amino-3-(diphenylamino)propan-2-ol (16a). ^1H NMR (400 MHz, CDCl_3) δ 7.22 (t, $J = 7.6$ Hz, 4H), 7.00 (d, $J = 7.8$ Hz, 4H), 6.93 (t, $J = 7.1$ Hz, 2H), 3.88 (m, 1H), 3.70 (d, $J = 6.0$ Hz, 2H), 2.94 (m, 3H), 2.83 (d, $J = 12.3$ Hz, 1H), 2.67–2.53 (m, 1H). ^{13}C NMR (101 MHz, CDCl_3) δ 148.35 (2C), 129.40 (4C), 121.81 (2C), 121.30 (4C), 68.86, 56.45, 44.57.

(S)-1-Amino-3-(diphenylamino)propan-2-ol (16b). ^1H NMR (400 MHz, CDCl_3) δ 7.22 (t, $J = 7.6$ Hz, 4H), 7.00 (d, $J = 7.8$ Hz, 4H), 6.93 (t, $J = 7.1$ Hz, 2H), 3.88 (m, 1H), 3.70 (d, $J = 6.0$ Hz, 2H), 2.94 (m, 3H), 2.83 (d, $J = 12.3$ Hz, 1H), 2.67–2.53 (m, 1H). ^{13}C NMR (101 MHz, CDCl_3) δ 148.35 (2C), 129.40 (4C), 121.81 (2C), 121.30 (4C), 68.86, 56.45, 44.57.

(R)-1-Amino-3-(diphenylamino)propan-2-ol (16c). ^1H NMR (400 MHz, CDCl_3) δ 7.22 (t, $J = 7.6$ Hz, 4H), 7.00 (d, $J = 7.8$ Hz, 4H), 6.93 (t, $J = 7.1$ Hz, 2H), 3.88 (m, 1H), 3.70 (d, $J = 6.0$ Hz, 2H), 2.94 (m, 3H), 2.83 (d, $J = 12.3$ Hz, 1H), 2.67–2.53 (m, 1H). ^{13}C NMR (101 MHz, CDCl_3) δ 148.35 (2C), 129.40 (4C), 121.81 (2C), 121.30 (4C), 68.86, 56.45, 44.57.

General Procedure for the Synthesis of Compounds 11–13.

The reaction is summarized in Scheme 1. Compounds 16a–c were solubilized in 3 mL of dichloromethane, 500 μL of acetic acid was added, and the resulting mixture was stirred at room temperature for 6 h. The solvent was removed under vacuum, and the resulting mixture was crystallized from acetonitrile.

1-Amino-3-(diphenylamino)propan-2-ol Acetate (11). Aspect white solid, $Y = 85\%$, ^1H NMR (400 MHz, D_2O) δ 7.29–7.25 (m, 4H), 7.01–6.96 (m, 6H), 4.16–4.01 (m, 1H), 3.82–3.71 (m, 2H), 3.15–3.11 (m, 1H), 2.892.83 (m, 1H), 1.84 (s, 3H). ^{13}C NMR (101 MHz, D_2O) δ 171.16, 148.35 (2C), 129.40 (4C), 121.81 (2C), 121.30 (4C), 68.86, 56.45, 44.57, 23.12 ppm.

(S)-1-Amino-3-(diphenylamino)propan-2-ol Acetate (12). Aspect white solid, $Y = 90\%$, ^1H NMR (400 MHz, D_2O) δ 7.29–7.25 (m, 4H), 7.01–6.96 (m, 6H), 4.16–4.01 (m, 1H), 3.82–3.71 (m, 2H), 3.15–3.11 (m, 1H), 2.892.83 (m, 1H), 1.84 (s, 3H). ^{13}C NMR (101 MHz, D_2O) δ 171.16, 148.35 (2C), 129.40 (4C), 121.81 (2C), 121.30 (4C), 68.86, 56.45, 44.57, 23.12 ppm.

(R)-1-Amino-3-(diphenylamino)propan-2-ol Acetate (13). Aspect white solid, $Y = 87\%$, ^1H NMR (400 MHz, D_2O) δ 7.29–7.25 (m, 4H), 7.01–6.96 (m, 6H), 4.16–4.01 (m, 1H), 3.82–3.71 (m, 2H), 3.15–3.11 (m, 1H), 2.892.83 (m, 1H), 1.84 (s, 3H). ^{13}C NMR (101 MHz, D_2O) δ 171.16, 148.35 (2C), 129.40 (4C), 121.81 (2C), 121.30 (4C), 68.86, 56.45, 44.57, 23.12 ppm.

Site-Directed Mutagenesis. The double mutant E256A/R262A was obtained from Biofab Research SRL (Rome, Italy) and cloned into a pET30a (Novagen) expression vector. The two single mutants E256A and R262A were obtained by site-directed mutagenesis as described.³⁹

Specifically, the DDX3X double mutant E256A/R262A cDNA cloned into pET30a was used to obtain the single mutants. Couples of primers of 36/42 bp overlapping for the whole length, except for a nucleotide, were used that revert one of the two alanines into the previous wild-type amino acid. To quickly verify the introduction of the correct mutation, a restriction site of SfiI was removed from the gene sequence of single mutants, without introducing any additional amino acid substitution.

The sequences of the primers were as follows (primer–primer overlapping sequences are underlined):

E256A fw: 5' tatgggcccgaacaataccaatctccttggtattagca 3'

E256A rv: 5' gcgccgccatctcctcattggccttcattgacct 3'

R262Afw: 5' atgaaggaataatggaaggtatgggcccgaacaaca 3'

R262A rv: 5' atttccttcattgcctcaagcctcgcctgacc 3'

The mutagenesis was carried out in the following reaction mixture: Pfu buffer 1 \times (Promega), dNTPs 0.2 mM, primers 1 μM , and 3 U of Pfu (Promega).

The polymerase chain reaction (PCR) cycles were as follows: 94 $^\circ\text{C}$ for 2 min (to denature the template DNA), and three amplification cycles at 94 $^\circ\text{C}$ for 1 min, 62 $^\circ\text{C}$ for 1 min, and 68 $^\circ\text{C}$ for 12 min. After that, an additional 12 amplification cycles were performed as follows: 94 $^\circ\text{C}$ for 1 min, 57 $^\circ\text{C}$ for 1 min, and 68 $^\circ\text{C}$ for 12 min. The PCR cycles were followed by an extension step at 68 $^\circ\text{C}$ for 60 min.

The PCR products were treated with 10 units of *DpnI* (Promega) at 37 $^\circ\text{C}$ for 2 h and then 10 μL of each PCR reaction was analyzed by agarose gel electrophoresis.

Amplified DNA was transformed into *Escherichia coli* DH5 α competent cells by heat shock following the standard protocol. The transformed cells were spread on an LB plate containing 50 $\mu\text{g}/\mu\text{L}$ Kanamycin and incubated at 37 $^\circ\text{C}$ overnight. Colonies from each plate were grown and the plasmid DNA was isolated. To verify the mutations, 400 ng of plasmid DNA was first linearized with 10 units of Hind III (Promega) for 1 h at 37 $^\circ\text{C}$ and then digested with 12 units of Sfi I (New England Biolabs) for 5 h at 50 $^\circ\text{C}$. Positive colonies were sent to Eurofins Genomics (Ebersberg, Germany) for Sanger sequencing to verify correct mutation insertions.

Protein Production and Purification. Purification of human recombinant full-length DDX3X was performed as described.²⁶ Briefly, DDX3X cDNA was cloned in the *E. coli* expression vector pET-30a(+). ShuffleT7 *E. coli* cells were transformed with the plasmid and grown at 37 $^\circ\text{C}$ up to $\text{OD}_{600} = 0.7$. DDX3X expression was induced with 0.5 mM IPTG at 15 $^\circ\text{C}$ O/N. Cells were harvested by centrifugation, lysed, and the crude extract was centrifuged at 100 000g for 60 min at 4 $^\circ\text{C}$ in a Beckman centrifuge before being loaded onto an FPLC Ni-NTA column (GE Healthcare). The column was equilibrated in buffer A (50 mM Tris-HCl pH 8.0, 250 mM NaCl, 25 mM imidazole, and 20% glycerol). After extensive washing in buffer A, the column was eluted with a linear gradient in buffer A from 25 to 250 mM imidazole. Proteins in the eluted fractions were visualized on sodium dodecyl sulfate-polyacrylamide gel electrophoresis (SDS-PAGE) and tested for the presence of DDX3X by Western blot with anti-DDX3X A300-474A (Bethyl Laboratories) at a 1:4000 dilution in 5% milk. Fractions containing the purest DDX3X protein were pooled and dialyzed in Slide-A-Lyzer MINI Dialysis Devices 20K MWCO (Thermo Scientific) for 3 h (25 mM Tris-HCl pH 8.0, 0.5 mM dithiothreitol (DTT), 100 mM NaCl, glycerol 20%) to remove excess salt. Finally, proteins were stored at -80 $^\circ\text{C}$.

The double-mutant protein E256A/R262A and the single mutants E256A and R262A were cloned in the *E. coli* expression vector pET-30a(+) and BL21(DE3) cells were transformed with the plasmids. Protein induction and purification were the same as those for the full-length protein. Only the double mutant E256A/R262A was dialyzed as the wild-type enzyme, whereas the single mutants E256A and R262A were maintained in elution buffer, avoiding further loss of material due to the dialysis procedure.

Helicase Assay Based on Fluorescence Resonance Energy Transfer (FRET). The FRET helicase assay was performed as described.¹⁵ Briefly, the dsRNA substrate for the helicase assay was prepared by hybridizing two ss RNA oligonucleotides with the following sequences:

Fluo-FAM: 5' UUUUUUUUUUUUUUUAGUACCGCCACCCU-CAGAACC 3'

Qu-BHQ1: 5' GGUUCUGAGGGUGGCGGUACUA 3'

DNA capture: 5' TAGTACCGCCACCCTCAGAACC 3'

The sequence in Fluo-FAM complementary to Qu-BHQ1 is underlined. Fluo-FAM carries a 6-carboxyfluorescein fluorophore at its 3' end, while Qu-BHQ1 carries a Black Hole quencher group at its 5' end. The DNA capture oligonucleotide is complementary to the Qu-BHQ1 oligonucleotide but bears no modifications.

Helicase assay using the dsRNA substrate was performed in 20 mM Tris-HCl (pH 8), 70 mM KCl, 2 mM MgCl_2 , 2 mM dithiothreitol, 12 units of RNasin (Promega), 2 mM ATP, 50 nM dsRNA, and 100 nM capture strand in 20 μL of reaction volume. The unwinding

reaction was started by adding 60 pmols of DDX3X recombinant protein and carried out at 37 °C for 40 min using a LightCycler 480 (Roche). The fluorescence intensity was recorded every 30 s. Data of fluorescence signals were analyzed by linear interpolation and the corresponding slope values were used to determine the apparent unwinding rate. The same assay was used to test all of the inhibitor molecules against DDX3X helicase activity. In the negative controls, we replaced the enzyme with dialysis buffer and the inhibitor with dimethyl sulfoxide (DMSO). In the positive control, the inhibitor is replaced with DMSO to detect the unwinding activity of the DDX3X enzyme only. This latter activity was taken as 100% enzymatic activity and compared to enzymatic activities in the presence of different inhibitor concentrations to calculate ID_{50} values.

ATPase Assay. The ATPase activity was determined, as previously described,¹¹ by directly monitoring (γ -32P) ATP hydrolysis by thin-layer chromatography (TLC). (γ -32P) ATP (3000 Ci/mmol) and TLC PEI Cellulose F plates were purchased from Hartmann Analytic and Merck, respectively.

The reaction was carried out in a final volume of 5 μ L, which contained different amounts of DDX3X proteins as specified in the figure legends, 0.1 μ M (γ -32P) of ATP (3000 Ci/mmol) as tracer plus 1 μ M of cold ATP, 5 mM $MgCl_2$, and nucleic acids as indicated. Samples were incubated for 30 min at room temperature and 1.5 μ L of the reaction was dotted onto TLC sheets of polyethylenimine cellulose. The products were separated by ascending chromatography with 0.5 M KH_2PO_4 (pH 3.4). The intensities of the radioactive bands corresponding to ATP and Pi were quantified by densitometric scanning with PhosphoImager (Typhoon, Ge Healthcare).

The ATPase activity was also determined using the commercial kit ADP-Glo Kinase Assay (Promega) as previously described.¹⁵ The reaction was performed in 30 mM Tris-HCl pH 8, 9 mM $MgCl_2$, 0.05 mg/mL BSA, 50 μ M ATP, and nucleic acids as indicated and different amounts of DDX3X proteins specified in the figures. The reaction was performed following the ADP-Glo Kinase Assay Protocol and luminescence was measured with MicroBetaTriLux (PerkinElmer).

Kinetic Analysis. Data (in triplicate) were plotted and analyzed by least-squares nonlinear regression with the computer program GraphPad Prism 6.0. Data were fitted to the following equation

$$v = V_{max}/(1 + (K_m/[S]^n)) \quad (1)$$

where v is the apparent reaction velocity at each substrate concentration, V_{max} is the maximum rate of the reaction, K_m is the Michaelis–Menten constant, S is the variable substrate concentration, and n is an exponential term to take into account sigmoidal dose–response curves, due to the positive cooperativity of DDX3X binding to RNA.⁴⁰

The turnover constant k_{cat} was calculated as $V_{max}/(\text{enzyme concentration})$ and the RNA substrate-binding efficiency of our enzymes was calculated as the k_{cat}/K_m ratio.

For the inhibition assays, the IC_{50} values have been calculated from dose–response curves. Data (in triplicate) were plotted and analyzed by least-squares nonlinear regression, according to the method of Marquardt–Levenberg, with the computer program GraphPad Prism 6.0. Data were fitted to the following equation

$$E_{obs} = E_{max}/(1 + (IC_{50}/[I])^n) \quad (2)$$

where $E_{(obs)}$ is the observed enzymatic activity in the presence of each inhibitor dose $[I]$, $E_{(max)}$ is the maximal enzymatic activity in the absence of the inhibitor, and n is an exponential term to take into account sigmoidal dose–response curves.

Cell Lines and Viruses. The human hepatoma cell line Huh7 (kindly provided by Istituto Toscano Tumori, Core Research Laboratory, Siena, Italy) and the African green monkey kidney cell line Vero E6 (ATCC no. CRL-1586) were cultured in high-glucose Dulbecco's modified Eagle's medium with sodium pyruvate and L-glutamine (DMEM; Euroclone) supplemented with 10% fetal bovine serum (FBS; Euroclone) and 1% penicillin/streptomycin (Pen/Strep, Euroclone) and incubated at 37 °C in a humidified incubator supplemented with 5% CO_2 . The *A. albopictus* mosquito cell line C6/

36 (ATCC no. CRL-1660) was cultured in DMEM as Huh7 and Vero E6 with additional L-glutamine (Euroclone, final concentration 6 mM) and 4-(2-hydroxyethyl)-1-piperazineethanesulfonic acid (HEPES; Euroclone, final concentration 25 mM) and incubated at 28 °C. The New Guinea C DENV serotype 2 strain was used for all of the experiments described in this work and was kindly provided by the Istituto Superiore di Sanità, Rome, Italy. The DENV strain was propagated in C6/36 cells and titrated by the plaque assay in Vero E6. The WNV (strain of lineage 2, kindly provided by Istituto Superiore di Sanità, Rome, Italy) viral stock, consisting of cell-free supernatants of acutely infected Huh7 cells, was aliquoted and stored at -80 °C until used. Titration of the viral stocks as plaque-forming units (PFUs) was carried out in Huh7 cells.

Cytotoxicity Assay—MTT. Monolayers of 2.5×10^4 Huh7 cells per well were added in flat-bottom 96-well culture plates and allowed to adhere overnight. Then, when the cell layers were confluent, the medium was removed, the wells were washed twice with phosphate buffered saline (PBS), treated with 100 μ L of DMEM with 10 μ L of DMSO alone (cell positive control), or with serial 10-fold dilutions of DDX3X inhibitors (final concentrations of 100, 10, 1, 0.1, and 0.01 μ M), and incubated for 3 days at 37 °C in a CO_2 . After treatment, an 3-(4,5-dimethylthiazol-2-yl)-2,5-diphenyltetrazolium bromide (MTT) kit (Roche, Milan, Italy) was used according to the supplier's instructions, and the absorbance of each well was determined using a microplate spectrophotometer at a wavelength of 570 nm. Cytotoxicity was calculated by dividing the average optical density of treated samples by the average of DMSO-treated samples (cell positive control).

Cytotoxicity Assays—CellTiter-Glo. Ribavirin (1- β -D-ribofuranosyl-1,2,4-triazole-3-carboxamide; Sigma-Aldrich cat. R9644), used as a reference compound, was supplied as a powder and dissolved in 100% dimethyl sulfoxide (DMSO).

The cytotoxicity of investigational compounds was determined by incubating 7000 Huh7 cells/well in the presence of serial 2-fold dilution of compounds. Similarly, dilutions of DMSO were added to cells to evaluate the cytotoxicity of the solvent used to resuspend tested compounds. After 72 h incubation, cells were treated with the CellTiter-Glo 2.0 Luminescent Cell Viability Assay (Promega) according to the manufacturer's protocol. The luminescence values obtained from cells treated with investigational compounds or DMSO were measured through the GloMax Discover Multimode Microplate Reader (Promega) and elaborated with the GraphPad PRISM software version 6.0 (La Jolla, California) to calculate the half-maximal cytotoxic concentration (CC_{50}).

WNV Inhibitory Viral Plaque Reduction Assay. Huh7 cells were used for the inhibitory viral plaque reduction assay. WNV was used to infect the Huh7 cell line in duplicate and viral plaques were visualized 4 days following infection. Briefly, 6-well plates were seeded with 2.5×10^5 cells in 3 mL of growth medium and kept overnight at 37 °C with 5% CO_2 . On the day of infection, after removal of growth medium, cell monolayers at 80–90% confluence were infected with the WNV viral stock with a multiplicity of infection (MOI) of 0.1 in a final volume of 0.3 mL and incubated for 1 h at 37 °C with 5% CO_2 . Then, cells were washed with PBS 1 \times , and 30 mL of dimethyl sulfoxide (DMSO) alone (viral positive control) or with 10-fold serial dilutions of DDX3X inhibitory compounds were immediately added in duplicate together with 300 mL of fresh DMEM complete medium (compound final concentrations of 100, 10, 1, 0.1, and 0.01 μ M). Ribavirin (1- β -D-ribofuranosyl-1,2,4-triazole-3-carboxamide; SIGMA) diluted in DMSO was used as an inhibitory reference control. Then, the overlay medium composed of 0.5% SeaPlaque Agarose (Lonza, Basel, Switzerland) diluted in propagation medium was added to each well. After 4 days (Huh7) of incubation at 37 °C, the monolayers were fixed with methanol (Carlo Erba Chemicals, Milan, Italy) and stained with 0.1% crystal violet (Carlo Erba Chemicals) and the viral titers were calculated by plaque-forming unit (PFU) counting. Percent of plaque reduction activity was calculated by dividing the average PFU of treated samples by the average of DMSO-treated samples (viral positive control). Fifty percent inhibitory concentrations (IC_{50}) were calculated using the predicted exponential growth

function in Microsoft Excel, which uses existing x - y data to estimate the corresponding anti-DDX3X compound concentration (x) from a known value (y), which, in this case, was 50% PFU. Mean $IC_{50} \pm$ standard deviations (SD) were calculated using all replicates. All experiments were repeated at least twice and all experimental procedures were conducted under biosafety level 3 containment.

DENV Immunodetection Assay. The immunodetection assay (IA) was designed to determine the antiviral activity of candidate antivirals on the whole viral replication cycle.⁴¹ Briefly, 7000 Huh7/well were infected with 50 TCID₅₀ of DENV. Viral adsorption was performed in 96-well plates for 1 h at 37 °C with 5% CO₂ and after virus removal, serial dilutions of each compound tested were added to the cells and incubated at 37 °C with 5% CO₂. In each test, ribavirin was used as control of the inhibition of viral replication, and infected and uninfected cells without drugs were used to calculate 100 and 0% of viral replication, respectively. After 72 h, supernatants were harvested and triplicate dilutions of generated viruses were used to infect preseeded Huh7 cells (7000 cells/well) for 72 h at 37 °C with 5% CO₂.

The supernatants were removed and cells were fixed for 30 min with 10% formaldehyde (Carlo Erba), rinsed with 1% PBS, and permeabilized for 10 min with 1% Triton X-100 (Carlo Erba). Cells were washed with PBS containing 0.05% Tween 20 (Carlo Erba) and incubated for 1 h with monoclonal anti-flavivirus mouse antibody (clone D1-4G2-4-15; Novus Bio) diluted 1:400 in blocking buffer (PBS containing 1% BSA and 0.1% Tween 20). After washing, cells were incubated for 1 h with a polyclonal horseradish peroxidase (HRP)-coupled anti-mouse IgG secondary antibody (Novus Bio NB7570) diluted 1:10 000 in blocking buffer. Next, cells were washed and the 3,3',5,5'-tetramethylbenzidine substrate (TMB, Sigma-Aldrich) was added to each well. After 15 min of incubation in the dark, the TMB peroxidase-based reaction was stopped with one volume of 0.5 M sulfuric acid. All incubation steps were performed at room temperature. Absorbance was measured at 450 nm optical density (OD₄₅₀) using the Absorbance Module of the GloMax Discover Multimode Microplate Reader (Promega).

Each IA run was validated by the OD₄₅₀ value above 1 in the virus control culture. OD₄₅₀ values from each well were normalized according to 100 and 0% of viral replication and normalized values were used to calculate half-maximal inhibitory concentration (IC_{50}) values through a nonlinear regression analysis of the dose–response curves generated with GraphPad PRISM software version 6.0.

■ ASSOCIATED CONTENT

Supporting Information

The Supporting Information is available free of charge at <https://pubs.acs.org/doi/10.1021/acs.jmedchem.0c01039>.

Molecular modeling MMGBSA procedure; binding energy of the ligand–receptor complex; homology model; purified recombinant proteins; kinetic of antiviral activities and cytotoxicity (PDF)

Molecular formula strings (CSV)

DDX3_homology_model (PDB)

■ AUTHOR INFORMATION

Corresponding Author

Giovanni Maga – Istituto di Genetica Molecolare IGM-CNR
“Luigi Luca Cavalli-Sforza”, I-27100 Pavia, Italy;
orcid.org/0000-0001-8092-1552; Email: giovanni.maga@igm.cnr.it

Authors

Valentina Riva – Istituto di Genetica Molecolare IGM-CNR
“Luigi Luca Cavalli-Sforza”, I-27100 Pavia, Italy
Anna Garbelli – Istituto di Genetica Molecolare IGM-CNR
“Luigi Luca Cavalli-Sforza”, I-27100 Pavia, Italy

Annalaura Brai – Dipartimento Biotechnologie, Chimica e Farmacia, Università degli Studi di Siena, I-53100 Siena, Italy;
orcid.org/0000-0001-6395-9348

Federica Casiraghi – Istituto di Genetica Molecolare IGM-CNR
“Luigi Luca Cavalli-Sforza”, I-27100 Pavia, Italy

Roberta Fazi – Dipartimento Biotechnologie, Chimica e Farmacia, Università degli Studi di Siena, I-53100 Siena, Italy

Claudia I. Trivisani – Dipartimento Biotechnologie, Chimica e Farmacia, Università degli Studi di Siena, I-53100 Siena, Italy

Adele Boccuto – Dipartimento di Biotechnologie Mediche, Università degli Studi di Siena, I-53100 Siena, Italy

Francesco Saladini – Dipartimento di Biotechnologie Mediche, Università degli Studi di Siena, I-53100 Siena, Italy;
orcid.org/0000-0002-9934-377X

Ilaria Vicenti – Dipartimento di Biotechnologie Mediche, Università degli Studi di Siena, I-53100 Siena, Italy

Francesco Martelli – Dipartimento di Medicina Sperimentale e Clinica, Università degli Studi di Firenze, I-50134 Firenze, Italy

Maurizio Zazzi – Dipartimento di Biotechnologie Mediche, Università degli Studi di Siena, I-53100 Siena, Italy

Simone Gianecchini – Dipartimento di Medicina Sperimentale e Clinica, Università degli Studi di Firenze, I-50134 Firenze, Italy

Elena Dreassi – Dipartimento Biotechnologie, Chimica e Farmacia, Università degli Studi di Siena, I-53100 Siena, Italy

Maurizio Botta – Dipartimento Biotechnologie, Chimica e Farmacia, Università degli Studi di Siena, I-53100 Siena, Italy;

Biotechnology College of Science and Technology, Temple University, Philadelphia, Pennsylvania 19122, United States;

orcid.org/0000-0003-0456-6995

Complete contact information is available at:
<https://pubs.acs.org/10.1021/acs.jmedchem.0c01039>

Author Contributions

V.R., A.G., and A.B. contributed equally to this work and should be considered as joint first authors. G.M. and M.B. had the original idea, secured funding, and supervised the work together with E.D. V.R., and A.G. purified DDX3X and planned and performed all of the enzymatic assays. F.C. contributed to the enzymatic assays. A.B., R.F., and C.I.T. designed the compounds. A.B. synthesized the compounds. A.Bo., F.S., I.V., and M.Z. planned and performed cell-based assays with DENV. F.M. and S.G. planned and performed cell-based assays with WNV. V.R. wrote the manuscript together with G.M., with the help of A.B. and A.G.

Funding

G.M. and V.R. were partially supported by the CNR Project “Identification of novel molecules with therapeutic potential against Zika virus and other emerging viruses”.

Notes

The authors declare no competing financial interest.

■ ACKNOWLEDGMENTS

This work is dedicated to the memory of Prof. Maurizio Botta, who was a founder and a leading mind of this project and passed his devotion for science to generations of researchers.

■ DEDICATION

[∇]Deceased, August 2nd, 2019.

■ ABBREVIATIONS

DENV, Dengue virus; WNV, West Nile virus; JEV, Japanese encephalitis virus; CHIKV, Chikungunya virus; ZIKV, Zika virus; DDX3X, human X-linked DEAD-box protein 3; HIV-1, human immunodeficiency virus type 1; HCV, hepatitis C virus; UM, unique motif; DDX1, human DEAD-box protein 1; STRS2, stress response suppressor 2; NS3, HCV nonstructural protein 3; PDGFR, platelet-derived growth factor receptor

■ REFERENCES

(1) Lindgren, E.; Andersson, Y.; Suk, J. E.; Sudre, B.; Semenza, J. C. Public health. Monitoring EU emerging infectious disease risk due to climate change. *Science* **2012**, *336*, 418–419.

(2) Forterre, P. The virocell concept and environmental microbiology. *ISME J.* **2013**, *7*, 233–236.

(3) Panda, D.; Cherry, S. Cell-based genomic screening: elucidating virus-host interactions. *Curr. Opin. Virol.* **2012**, *2*, 784–792.

(4) Soto-Rifo, R.; Rubilar, P. S.; Ohlmann, T. The DEAD-box helicase DDX3 substitutes for the cap-binding protein eIF4E to promote compartmentalized translation initiation of the HIV-1 genomic RNA. *Nucleic Acids Res.* **2013**, *41*, 6286–6299.

(5) Ariumi, Y. Multiple functions of DDX3 RNA helicase in gene regulation, tumorigenesis, and viral infection. *Front. Genet.* **2014**, *5*, No. 423.

(6) He, T.-Y.; Wu, D.-W.; Lin, P.-L.; Wang, L.; Huang, C.-C.; Chou, M.-C.; Lee, H. DDX3 promotes tumor invasion in colorectal cancer via the CK1 ϵ /Dvl2 axis. *Sci. Rep.* **2016**, *6*, No. 21483.

(7) Botlagunta, M.; Vesuna, F.; Mironchik, Y.; Raman, A.; Lisok, A.; Winnard, P.; Mukadam, S.; Van Diest, P.; Chen, J. H.; Farabaugh, P.; Patel, A. H.; Raman, V. Oncogenic role of DDX3 in breast cancer biogenesis. *Oncogene* **2008**, *27*, 3912–3922.

(8) Bol, G. M.; Xie, M.; Raman, V. DDX3, a potential target for cancer treatment. *Mol. Cancer* **2015**, *14*, No. 188.

(9) Kondaskar, A.; Kondaskar, S.; Fishbein, J. C.; Carter-Cooper, B. A.; Lapidus, R. G.; Sadowska, M.; Edelman, M. J.; Hosmane, R. S. Structure-based drug design and potent anti-cancer activity of tricyclic 5:7:5-fused diimidazo[4,5-d:4',5'-f][1,3]diazepines. *Bioorg. Med. Chem.* **2013**, *21*, 618–631.

(10) Bol, G. M.; Vesuna, F.; Xie, M.; Zeng, J.; Aziz, K.; Gandhi, N.; Levine, A.; Irving, A.; Korz, D.; Tantravedi, S.; Heerma van Voss, M. R.; Gabrielson, K.; Bordt, E. A.; Polster, B. M.; Cope, L.; van der Groep, P.; Kondaskar, R. S.; van der Wall, E.; van Diest, P. J.; Tran, P. T.; Raman, V.; et al. Targeting DDX3 with a small molecule inhibitor for lung cancer therapy. *EMBO Mol. Med.* **2015**, *7*, 648–669.

(11) Garbelli, A.; Beermann, S.; Di Cicco, G.; Dietrich, U.; Maga, G. A motif unique to the human dead-box protein DDX3 is important for nucleic acid binding, ATP hydrolysis, RNA/DNA unwinding and HIV-1 replication. *PLoS One* **2011**, *6*, No. e19810.

(12) Schröder, M. Viruses and the human DEAD-box helicase DDX3: inhibition or exploitation? *Biochem. Soc. Trans.* **2011**, *39*, 679–683.

(13) Schröder, M.; Baran, M.; Bowie, A. G. Viral targeting of DEAD box protein 3 reveals its role in TBK1/IKK ϵ -mediated IRF activation. *EMBO J.* **2008**, *27*, 2147–2157.

(14) Garbelli, A.; Riva, V.; Crespan, E.; Maga, G. How to win the HIV-1 drug resistance hurdle race: running faster or jumping higher? *Biochem. J.* **2017**, *474*, 1559–1577.

(15) Brai, A.; Fazi, R.; Tintori, C.; Zamperini, C.; Bugli, F.; Sanguinetti, M.; Stigliano, E.; Esté, J.; Badia, R.; Franco, S.; Martinez, M. A.; Martinez, J. P.; Meyerhans, A.; Saladini, F.; Zazzi, M.; Garbelli, A.; Maga, G. Human DDX3 protein is a valuable target to develop broad spectrum antiviral agents. *Proc. Natl. Acad. Sci. U.S.A.* **2016**, *113*, 5388–5393.

(16) Meier-Stephenson, V.; Mrozowich, T.; Pham, M.; Patel, T. R. DEAD-box helicases: the Yin and Yang roles in viral infections. *Biotechnol. Genet. Eng. Rev.* **2018**, *34*, 3–32.

(17) Cordin, O.; Banroques, J.; Tanner, N. K.; Linder, P. The DEAD-box protein family of RNA helicases. *Gene* **2006**, *367*, 17–37.

(18) Siegel, R.; Naishadham, D.; Jemal, A. Cancer statistics. *Ca-Cancer J. Clin.* **2013**, *63*, 11–30.

(19) Schütz, P.; Karlberg, T.; van den Berg, S.; Collins, R.; Lehtio, L.; Högbom, M.; Holmberg-Schiavone, L.; Tempel, W.; Park, H. W.; Hammarström, M.; Moche, M.; Thorsell, A. G.; Schüler, H. Comparative structural analysis of human DEAD-Box RNA helicases. *PLoS One* **2010**, *5*, No. e12791.

(20) Song, H.; Ji, X. The mechanism of RNA duplex recognition and unwinding by DEAD-box helicase DDX3X. *Nat. Commun.* **2019**, No. 3085.

(21) Oda, S.; Schröder, M.; Khan, A. R. Structural basis for targeting of human RNA helicase DDX3 by poxvirus protein K7. *Structure* **2009**, *17*, 1528–1537.

(22) Furuta, Y.; Takahashi, K.; Shiraki, K.; Sakamoto, K.; Smee, D. F.; Barnard, D. L.; Gowen, B. B.; Julander, J. G.; Morrey, J. D. T-705 (favipiravir) and related compounds: Novel broad-spectrum inhibitors of RNA viral infections. *Antiviral Res.* **2009**, *82*, 95–102.

(23) Wolf, M. C.; Freiberg, A. N.; Zhang, T.; Akyol-Ataman, Z.; Grock, A.; Hong, P. W.; Li, J.; Watson, N. F.; Fang, A. Q.; Aguilar, H. C.; Porotto, M.; Honko, A. N.; Damoiseaux, R.; Miller, J. P.; Woodson, S. E.; Chamtasirivisal, S.; Fontanes, V.; Negrete, O. A.; Krogstad, P.; Dasgupta, A.; Moscona, A.; Hensley, L. E.; Whelan, S. P.; Faull, K. F.; Holbrook, R.; Jung, M. E.; Lee, B. A broad-spectrum antiviral targeting entry of enveloped viruses. *Proc. Natl. Acad. Sci. U.S.A.* **2010**, *107*, 3157–3162.

(24) Hoffmann, H.-H.; Kunz, A.; Simon, V. A.; Palese, P.; Shaw, M. L. Broad-spectrum antiviral that interferes with de novo pyrimidine biosynthesis. *Proc. Natl. Acad. Sci. U.S.A.* **2011**, *108*, 5777–5782.

(25) Lee, S. J.; Wang, J. Y. J. Exploiting the promiscuity of imatinib. *J. Biol.* **2009**, *8*, No. 30.

(26) Brai, A.; Riva, V.; Saladini, F.; Zamperini, C.; Trivisani, C. I.; Garbelli, A.; Pennisi, C.; Giannini, A.; Boccutto, A.; Bugli, F.; Martini, M.; Sanguinetti, M.; Zazzi, M.; Dreassi, E.; Maga, G.; Botta, M. DDX3X inhibitors, an effective way to overcome HIV-1 resistance. *Eur. J. Med. Chem.* **2020**, *200*, No. 112319.

(27) Brai, A.; Martelli, F.; Riva, V.; Garbelli, A.; Fazi, R.; Zamperini, C.; Pollutri, A.; Falsitta, L.; Ronzini, S.; Maccari, L.; Maga, G.; Giannecchini, S.; Botta, M. DDX3X helicase inhibitors as a new strategy to fight the west Nile virus infection. *J. Med. Chem.* **2019**, *62*, 2333–2347.

(28) Riva, V.; Maga, G. From the magic bullet to the magic target: exploiting the diverse roles of DDX3X in viral infections and tumorigenesis. *Future Med. Chem.* **2019**, *11*, 1357–1381.

(29) Brai, A.; Boccutto, A.; Monti, M.; Marchi, S.; Vicenti, I.; Saladini, F.; Trivisani, C. I.; Pollutri, A.; Trombetta, C. M.; Montomoli, E.; Riva, V.; Garbelli, A.; Nola, E. M.; Zazzi, M.; Maga, G.; Dreassi, E.; Botta, M. Exploring the implication of DDX3X in DENV infection: discovery of the first-in-class DDX3X fluorescent inhibitor. *ACS Med. Chem. Lett.* **2020**, *11*, 956–962.

(30) Manni, M.; Guglielmino, C. R.; Scolari, F.; Vega-Rúa, A.; Failloux, A.-B.; Somboon, P.; Lisa, A.; Savini, G.; Bonizzoni, M.; Gomulski, L. M.; Malacrida, A. R.; Gasperi, G. Genetic evidence for a worldwide chaotic dispersion pattern of the arbovirus vector, *Aedes albopictus*. *PLoS Neglected Trop. Dis.* **2017**, *11*, No. e0005332.

(31) *Schrödinger Release 2014-3: Prime, Version 3.7*; Schrödinger, LLC: New York, NY, 2014.

(32) Sengoku, T.; Nureki, O.; Nakamura, A.; Kobayashi, S.; Yokoyama, S. Structural basis for RNA unwinding by the DEAD-box protein *Drosophila vasa*. *Cell* **2006**, *125*, 287–300.

(33) Högbom, M.; Collins, R.; Van den Berg, S.; Jenvert, R. M.; Karlberg, T.; Kotenyova, T.; Flores, A.; Karlsson Hedestam, G. B.; Schiavone, L. H. Crystal structure of conserved domains 1 and 2 of the human DEAD-box helicase DDX3X in complex with the mononucleotide AMP. *J. Mol. Biol.* **2007**, *1*, 150–159.

(34) *Schrödinger Release 2014-3: MacroModel, Version 10.5*; Schrödinger, LLC: New York, NY, 2014-3.

(35) *Small-Molecule Drug Discovery Suite 2014-3: Glide, Version 6.4*; Schrödinger, LLC: New York, NY, 2014.

(36) Jones, G.; Willett, P.; Glen, R. C. Molecular recognition of receptor sites using a genetic algorithm with a description of desolvation. *J. Mol. Biol.* **1995**, *245*, 43–53.

(37) *The PyMOL Molecular Graphics System, Version 1.5.0.4*; Schrödinger, LLC: New York, 2006.

(38) Pettersen, E. F.; Goddard, T. D.; Huang, C. C.; Couch, G. S.; Greenblatt, D. M.; Meng, E. C.; Ferrin, T. E. UCSF Chimera—a visualization system for exploratory research and analysis. *J. Comput. Chem.* **2004**, *25*, 1605–1612.

(39) Liu, H.; Naismith, J. H. An efficient one-step site-directed deletion, insertion, single and multiple-site plasmid mutagenesis protocol. *BMC Biotechnol.* **2008**, *8*, No. 91.

(40) Sharma, D.; Putnam, A. A.; Jankowsky, E. Biochemical differences and similarities between the DEAD-Box helicase orthologs DDX3X and Ded1p. *J. Mol. Biol.* **2017**, *429*, 3730–3742.

(41) Vicenti, I.; Dragoni, F.; Giannini, A.; Giammarino, F.; Spinicci, M.; Saladini, F.; Boccutto, A.; Zazzi, M. Development of a cell-based immunodetection assay for simultaneous screening of antiviral compounds inhibiting Zika and dengue virus replication. *SLAS Discovery* **2020**, *25*, 506–514.